ACS OMEGA

http://pubs.acs.org/journal/acsodf

Article

Preparation and Characterization of Additional Metallic Element-Containing Tubular Iron Oxides of Bacterial Origin

Katsunori Tamura,* Tatsuki Kunoh, Makoto Nakanishi, Yoshihiro Kusano, and Jun Takada*

Cite This: *ACS Omega* 2020, 5, 27287−27294

Read Online

ACCESS | Metrics & More | Article Recommendations | Supporting Information

ABSTRACT: Biogenic microtubular iron oxides (BIOXs) derived from *Leptothrix* spp. are known as promising multifunctional materials for industrial applications such as ceramic pigments and catalyst carriers. Here, we report unprecedented BIOX products with additive depositions of various metallic elements prepared by a newly devised "two-step" method using an artificial culture system of *Leptothrix cholodnii* strain OUMS1; the method comprises a biotic formation of immature organic sheaths and subsequent abiotic deposition of Fe and intended elements on the sheaths. Chemical composition ratios of the additional elements Al, Zr, and Ti in the respective BIOXs were arbitrarily controllable depending on initial concentrations of metallic salts added to reaction solutions. Raman spectroscopy exemplified an existence of Fe−O−Al linkage in the Al-containing BIOX matrices. Time-course analyses revealed the underlying physiological mechanism for the BIOX formation. These results indicate that our advanced method can contribute greatly to creations of innovative bioderived materials with improved functionalities.

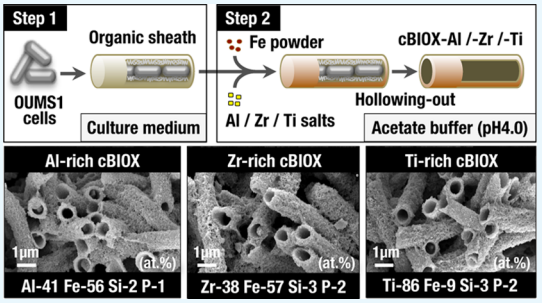

INTRODUCTION

Iron oxides are widespread compounds in nature, which include not only common mineral iron oxides generated by geological actions but also bioderived ones formed by metabolic actions of iron-oxidizing organisms. The latter exist especially in hydrosphere environments such as Fe/Mn-rich seeps and ferrous ion flows. In such areas, communities of iron-oxidizing bacteria precipitate ocherous masses consisting primarily of bacterial excretes (organic exopolymers) and iron hydroxides from the aqueous phase.[1,2] One of the most prominent groups of iron bacteria habiting in the wetlands are sheath-forming bacteria which, based on their remarkable morphology, were classified in the genera *Leptothrix* and *Sphaerotilus* and gained attention since the early days of microbiology.[3,4] *Leptothrix* species inhabit different types of aquatic environments, and, in general, produce Fe/Mn-rich, extracellular microtubular sheaths through interactions of their exopolymers containing saccharic and proteinaceous organics with aqueous-phase inorganics, in particular, at spring-fed zones. These sheaths referred to as biogenous iron oxides (BIOXs)[5] are the ingenious organic/inorganic hybrid constructs with an amorphous texture containing Fe, Si, P, and often Ca as major inorganic compounds. The *Leptothrix*-type BIOX (*L*-BIOX) sheaths with ferromanganese oxides hold promise as absorbents for removing hazardous metal ions from water because of their highly porous, amorphous, and heterogeneous nature.[6] Indeed, the ability to recruit Fe and Mn to *L*-BIOX sheaths has been applied for purification of facilities for groundwater.[7] In addition, their capacity for adsorption of other metals such as arsenic and lead and organics was found to be useful in water treatment schemes that promote the bacterial growth using natural Fe-rich waters.[8] Furthermore, with their unique physicochemical features such as micrometer-sized (in diameter) tubular structures with high specific surface area and porousness, bioinspired engineering has demonstrated that the *L*-BIOX sheaths are applicable to industrial materials, including porcelain red pigments,[9] anode materials for lithium-ion batteries,[10] and carriers of catalysts and enzymes.[11,12] Hence, there have been various proven functionalities for the *L*-BIOX sheaths; however, because the *L*-BIOXs are naturally occurring ready-made products, they have a definitive drawback in that it is virtually impossible to further improve the functionality by modifying the chemical composition and physical structures.

Isolation and axenic culture of some iron-depositing sheathed bacteria have, meanwhile, enabled us to investigate the microorganisms and the derived iron oxide sheaths through biochemical and physiological approaches under laboratory conditions. The representative strains isolated so far are assigned in species of genus *Leptothrix*, the heterotrophic sheathed bacteria belonging to the class of *Betaproteobacteria*.[7,13−15] Biochemical studies with *Leptothrix cholodnii*

Received: July 27, 2020
Accepted: October 2, 2020
Published: October 16, 2020

https://dx.doi.org/10.1021/acsomega.0c03574
ACS Omega 2020, 5, 27287−27294

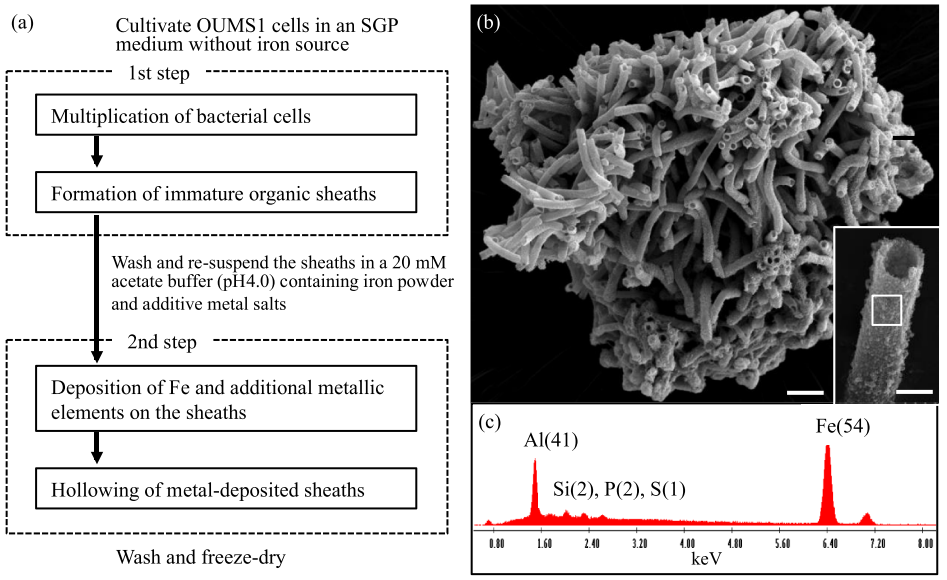

Figure 1. Preparation of additive metal-deposited BIOX sheaths. (a) Flow chart of experimental procedures and events (surrounded by rectangles). (b) SEM image of a clump of Al-deposited BIOX sheaths. The inset is the magnified image of a sheath tip. The white square denotes the representative area for EDX analysis. The scale bar is 10 μm (1 μm in the inset). (c) SEM−EDX spectrum. Each peak corresponds to the respective element, and numerical values (means, n = 8) in parentheses are elemental composition ratios (at. %).

(former *Leptothrix discophora*) strains revealed the chemical properties of the Fe-encrusted sheaths,[6,16] an important role of disulfide bonds in maintaining the sheath structure of strain SP-6,[17] and the enzymatic features of iron oxidation in a sheathless strain SS-1.[18] The other line of study using *L. cholodnii* strain OUMS1 elucidated the bacterial behaviors during tubular sheath formation,[19] the mode of sheath elongation for rapid massive production of sheaths,[20] and the mechanism for the abiotic deposition of iron oxides on sheaths.[21] Moreover, culture-based BIOX (referred to as cBIOX hereafter) sheaths have been investigated using bacterial strains of *Leptothrix* spp. from the perspective of material science.[22−25] Our previous study has demonstrated that the chemical compositions and crystallinity of cBIOX products can be modified by an alteration of Si concentrations in the culture medium.[26] The findings intriguingly suggested that there is plenty of scope for desired improvements in the cBIOXs as highly functional materials according to the industrial demand.

In general, an additional sorption of specific metal elements in inorganic materials is expected to lead to an improvement of the functionality or a creation of innovative functions. However, few studies have so far focused on changes in chemical compositions of the BIOX by an addition of metallic elements, which are originally uncontained. In this study, we therefore addressed in creating novel BIOXs, which contain additional metallic elements by utilizing their ability to deposit various metallic elements on the sheaths. For example, inclusions of Al and Zr in BIOX materials are predicted to be applicable for thermostable pigments and highly active catalysts, and Ti-containing BIOXs will be useable as effective scaffolding materials for cell cultures and high-performance photocatalysts. Several lines of evidence indicated that iron sources are not absolutely necessary for the growth and sheath formation of certain strains in *L. cholodnii*[27,28] and that the depositions of iron oxides onto immature organic sheaths do not require the living bacterial cells.[21,29] Based on the findings, we divided the conventional culture system into two consecutive processes comprising a formation of immature organic sheaths and a deposition of metal oxides onto the sheaths.

RESULTS AND DISCUSSION

Upon preparing BIOX sheaths containing additional metallic elements by the conventional culture method, we were concerned about two possible obstacles including toxicity of certain metals against the bacterial growth and solubility of metal salts in the culture medium. We thus first examined inhibitory effects of several metallic salts on the growth of OUMS1 cells. Results showed that Al and Ru inhibited the growth at concentrations of more than 5 mM and 0.5 mM, respectively, in contrast to Si, a constituent of the culture medium that did not affect the growth at all concentrations tested (Figure S1). We therefore devised a novel "two-step" method, consisting of the bacterial culture-based formation of primary nonferrous organic sheaths in the early stationary phase and abiotic deposition of metal elements on the sheath, an outline flow of which is shown in Figure 1a. Notably, in the second step, 20 mM acetate buffer (pH 4.0) was used to ensure the solubility of additive metal salts. Besides, the usage of the acidic buffer solution, unlike the ordinary culture medium with a neutral pH range, created suitable conditions in which Fe ions were gradually dissolved from iron powder and oxidized (Figure S2).

With the use of the two-step method, Al-deposited cBIOX (hereafter abbreviated as cBIOX-Al) was successfully obtained as clumps of a large number of hollow sheaths, each of which had a microtubular form with an outer diameter of ∼1.0 μm and an inner diameter of ∼0.8 μm (Figure 1b). The morphological features of the sheath were similar to those of the OUMS1-derived BIOXs which were prepared by a different method.[23] Unlike *L*-BIOX sheaths, most of which are obtained as separate tubes, the sheath clumps were formed in the case of cBIOX, probably because of a gentle rotary shaking of the sheaths throughout the preparation method. Scanning electron microscopy (SEM)−energy-dispersive X-ray

https://dx.doi.org/10.1021/acsomega.0c03574
ACS Omega 2020, 5, 27287−27294

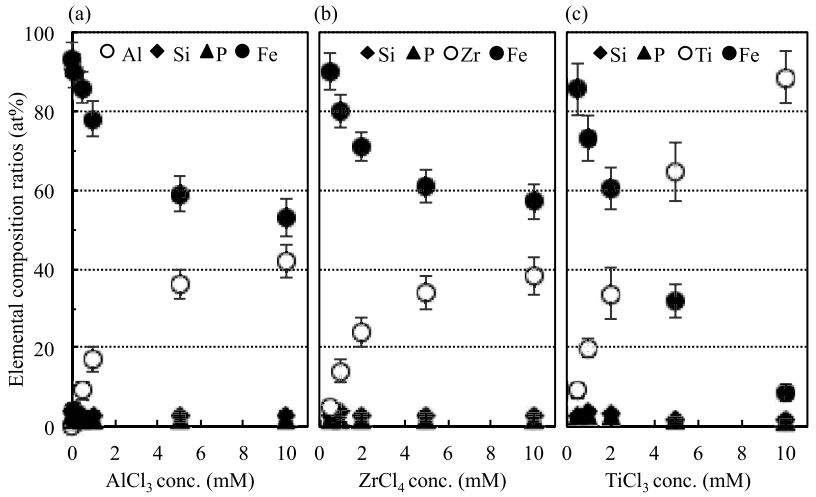

Figure 2. Relationships between concentrations of additive metallic salts in iron deposition solutions and elemental composition ratios in sheath products. (a–c) Elemental composition ratios in the BIOX products prepared with various concentrations of $AlCl_3$ (a), $ZrCl_4$ (b), and $TiCl_3$ (c) in iron deposition solutions, determined by SEM–EDX analysis. The additive elements Al, Zr, and Ti are represented by open circles. Other major elements Fe, Si, and P are denoted by closed circles, closed diamonds, and closed triangles, respectively. Plotted data are the means (n = 8), and vertical bars indicate the SD.

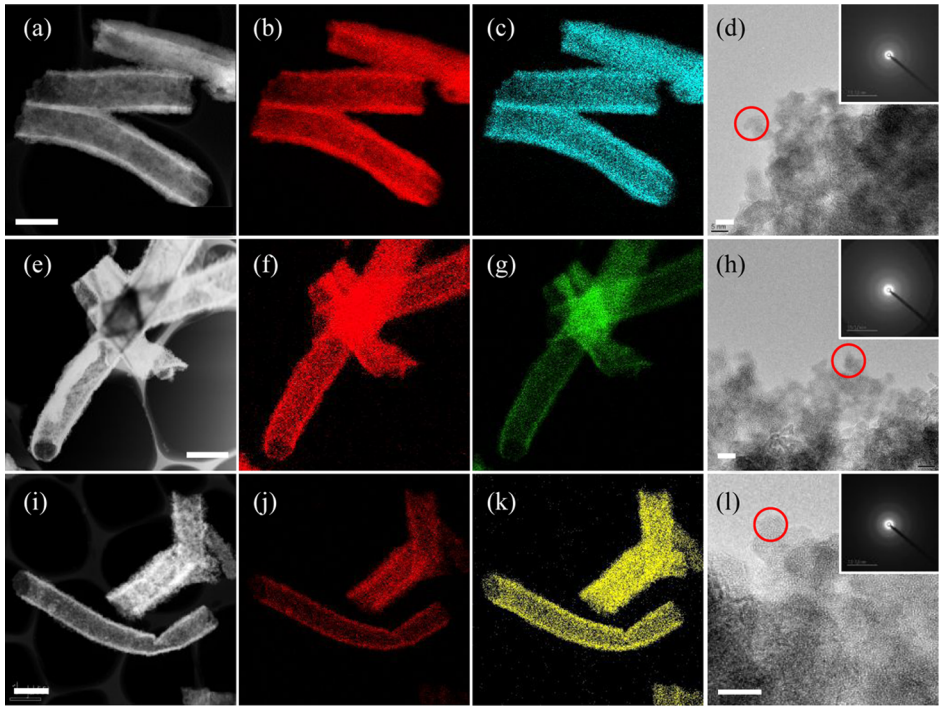

Figure 3. Microstructure, elemental distribution, and crystallinity of additive metal-deposited BIOX sheaths. HAADF images (the leftmost column), elemental mapping images (the second and third columns from the left), and TEM images of the outer surface (the rightmost column) for Al (a–d)-, Zr (e–h)-, and Ti (i–l)-deposited sheath products. In the elemental maps, Fe, Al, Zr, and Ti are shown in red, blue, green, and yellow, respectively. The scale bars are 1 μm in the HAADF images and 5 nm in the TEM images. Insets in the TEM images are ED patterns for the areas indicated with red circles.

spectrometry (EDX) analysis showed that the composition ratios (at. %) of major elements in the cBIOX-Al sheaths were Al/Fe/Si/P/S = 41:54:2:2:1 when prepared with 10 mM $AlCl_3$ in the iron deposition solution (Figure 1c). An average yield of the dried cBIOX-Al products was estimated to be 800 mg mL^{-1}, which was obtained by dividing the dry weight of the final product by the volume of the culture fluid in the first step. In addition, using $ZrCl_4$ and $TiCl_3$ as the additive metal salts, Zr- and Ti-deposited cBIOXs (hereafter abbreviated as cBIOX-Zr and cBIOX-Ti, respectively) were also produced by the same two-step method. The micromorphology of the two metal-deposited BIOXs was nearly identical to that of cBIOX-Al (Figure S3a,b). The composition ratios (at. %) of cBIOX-Zr and cBIOX-Ti sheaths were Zr/Fe/Si/P/S = 38:56:3:2:1 and Ti/Fe/Si/P/S = 86:8:3:2:1, respectively, when prepared in the presence of $ZrCl_4$ and $TiCl_3$ at a concentration of 10 mM (Figure S3c,d).

https://dx.doi.org/10.1021/acsomega.0c03574
ACS Omega 2020, 5, 27287–27294

We next examined whether the concentrations of additive metal salts in the reaction (iron deposition) solution correspond to the composition ratios of the respective elements in the BIOX products. When the concentrations of $AlCl_3$ and $ZrCl_4$ increased in stages, the contents of Al and Zr in the respective products elevated along with a decrease in Fe contents, and both reached maximum levels of ∼40 at. % in the case that the metal salt concentrations were 10 mM (Figure 2a,b). Because the values of standard deviations for elemental composition ratios are relatively small, the Al- and Zr-deposited BIOX sheaths are considered to have a chemical homogeneity. These results thus indicate that the chemical composition of the BIOX sheaths can be controlled optionally by altering the concentrations of additive metallic salts in the iron deposition solution. On the other hand, although the increase in $TiCl_3$ concentrations similarly caused elevated levels of Ti contents and decreased Fe contents in the cBIOX-Ti products, it is noteworthy that the maximum value of Ti contents was a remarkably high level (∼85 at. %) when 10 mM $TiCl_3$ was used (Figure 2c). The result suggests that, unlike in the case of Al and Zr, Ti was deposited in the BIOX sheaths through an unknown manner, which is plausibly associated with a reductive dissolution of iron oxides by Ti(III) solution.[30]

STEM-EDS mapping analysis of cBIOX-Al40, cBIOX-Zr40, and cBIOX-Ti86 (the numbers of approximate values of the respective elemental composition ratios) revealed that the additionally deposited metals Al, Zr, and Ti are distributed nearly uniformly in the respective cBIOX sheaths in a segregation-free manner (Figure 3a−c,e−g,i−k). The microstructures and crystallinity were investigated by the TEM and electron diffraction (ED) analyses. Figure 3d,h,l shows that the basic textures of sheath surfaces in the three kinds of cBIOXs are composed of amorphous primary particles with a diameter of ∼5 nm because the respective ED patterns are typical concentric halos with two diffraction rings, which are characteristics of amorphous two-line ferrihydrite. It was thus indicated that the depositions of the additional metallic elements onto cBIOX sheaths had little influence on the microstructure and crystalline nature.

The crystallinity of the various Al-containing BIOX sheaths was evaluated by the powder XRD analysis. As shown in Figure 4, the increase in Al contents in BIOX products led to a transition from a crystal phase of goethite to amorphous ferrihydrite-like ferric oxyhydroxide, suggesting that Al contents can regulate the crystallinity of the BIOX sheaths. Likewise, XRD patterns of cBIOX-Zr40 and cBIOX-Ti86 showed amorphous aspects similar to the results from the ED analysis (Figure 3h,i). The situation resembles a previously reported case of Si, in which increased Si contents in the BIOX induced the phase transition from lepidocrocite to two-line ferrihydrite.[26] The cBIOX-Ti86 product is also referred to by an alternate name "titania microtubule (TMT)" because of the close similarity to amorphous titania, as shown by XRD analysis.

The specific surface area and pore size distribution were determined by measuring the nitrogen adsorption isotherms of cBIOX-Al, cBIOX-Zr, and cBIOX-Ti sheaths. The BET surface areas of cBIOX-Al20, cBIOX-Al40, cBIOX-Zr40, and cBIOX-Ti86/TMT were 151, 97, 75, and 56 $m^2\ g^{-1}$, respectively, while that of cBIOX (without additional metal depositions) was 184 $m^2\ g^{-1}$. It is assumed that the smaller BET surface area of cBIOX than that of *L*-BIOX (280 $m^2\ g^{-1}$)[11] is caused by

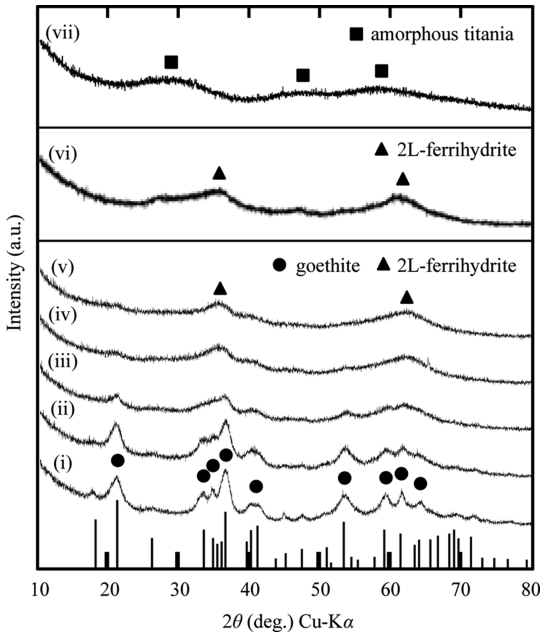

Figure 4. XRD spectroscopy of cBIOX-Al, cBIOX-Zr, and cBIOX-Ti samples. (i−v) XRD patterns of (i) cBIOX-Al0, (ii) -Al6, (iii) -Al15, (iv) -Al28, and (v) -Al40. (vi,vii) XRD spectra of (vi) cBIOX-Zr40 and (vii) cBIOX-Ti86. The vertical lines at the bottom represent the intensity ratios of goethite (JCPDS no. 29-0713). Typical patterns are indicated for goethite (closed circle), two-line ferrihydrite (closed triangle), and amorphous titania (closed square).

different sizes of primary particles and possibly by different thicknesses of microfibrils between the two types of BIOXs, which are produced in distinct nutrient environments. Besides, it was shown that the size distribution of mesopores in cBIOX-Al40 shifted to the smaller side (Figure S4a) and that those of micropores in cBIOX-Al40 converged to a size of 1.6 nm, unlike discrete size distributions (1.1 nm, 1.4 nm, and 1.7 nm) in cBIOX (Figure S4b). In addition, pore size distribution analysis of cBIOX-Zr40 and cBIOX-Ti86/TMT sheaths showed that mesopores and micropores were estimated to be both dp = 1.2 nm of mesopores and rp = 0.7 and 0.6 nm of micropores, respectively (Figure S5). Therefore, these results indicate that the deposition of Al, Zr, and Ti on BIOX sheaths tends to cause a decrease in specific surface area, which can be attributed primarily to the changes in pore size distributions, even though the Al-, Zr-, and Ti-containing BIOX sheaths still have a high porosity.

The chemical state of the additional metal element in the cBIOX sheaths was investigated by the Raman spectroscopic analysis. The result showed that a specific band near 710 cm^{-1} in cBIOX-Al40 shifted from the band near 696 cm^{-1} in non-Al-containing cBIOX (Figure 5). Liu et al. reported that the feature bands of goethite shifted to high wavenumbers after the occurrence of Al substitution for Fe in the structure of goethite.[31] According to the findings, it is possible that cBIOX-Al40 has partial substitution of Al for Fe, thereby containing a chemical linkage of Fe−O−Al in the amorphous matrix. In addition, we assume that the broader band near 400 cm^{-1} in cBIOX-Al40 reflects an amorphous state of the sample, as compared with the corresponding band of the cBIOX, which has a crystal phase of goethite (Figure 4). Consequently, we infer that the deposited Al onto the cBIOX sheaths sorbed by forming a chemical linkage with Fe via O in the fibrillar matrix

https://dx.doi.org/10.1021/acsomega.0c03574
ACS Omega 2020, 5, 27287−27294

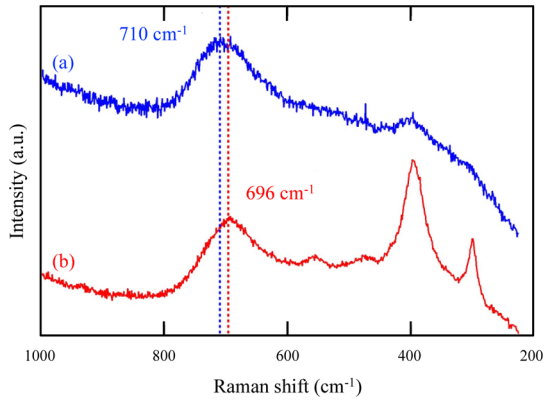

Figure 5. Raman spectroscopy of (a) Al (40 at. %)-containing and (b) non-Al-containing cBIOX sheaths. The positions of the respective specific peaks of the Raman shift are indicated with (a) blue and (b) red dotted lines.

but does not exist in manners of simple adhesion, accumulation, or adsorption. In the case of Zr-containing cBIOX, meanwhile, the specific band near 696 cm^{-1} for goethite shifted to the lower wavenumber side (near 657 cm^{-1}) in the Raman spectrum of cBIOX-Zr40 (Figure S6a), suggesting theoretically that Fe in cBIOX matrices was replaced by a larger mass number element Zr. Besides, because a convex segment including the goethite-specific band disappeared in the spectra of cBIOX-Ti50 and cBIOX-Ti86/TMT with high Ti contents (Figure S6b), it was thereby implied that Fe in cBIOX matrices was largely substituted with Ti.

To explore the underlying mechanisms involved in the deposition of metallic elements on immature organic sheaths and the formation of hollow sheaths, a time-course analysis was carried out using the experimental conditions optimized in this study. Results revealed that the cBIOX formation process is composed of the following four successive events: (i) untying of organic fibrils on primary immature sheaths, (ii) deposition of iron oxide nanoparticles on organic fibrils, (iii) swelling and hollowing out of sheath bodies, and (iv) weaving and compaction of iron-deposited fibrils into tubular sheaths (Figure 6). In the first event, organic fibrils weaved on an outer layer of primary sheaths were untied in the presence of eluted ferric ions and/or iron(II)−iron(III) hydroxides (Figure 6b,f, the second diagram from the left in Figure 6i), in accordance with the developing coloration of the solution to reddish brown (Figure S2). Considering that the disulfide bonds existing in the fibrils play an essential role in maintaining the structural integrity of the *Leptothrix* sheaths,[17] it was deduced that the untying of the organic fibrils arose from a cleavage of the disulfide bonds in the sheaths through a reducing ability of ferric ions and/or ferric hydroxide−ferrous hydroxide. The presumed contribution of the reductive cleavage of disulfide bonds to disentanglement of fibrils was supported partially by the results from biochemical experiments (Figure S7). The exposure of the organic fibrils appeared to promote a deposition of amorphous hydrous iron oxide compounds such as ferrihydrite, which seemed to adhere directly to the organic fibrils, as was reported

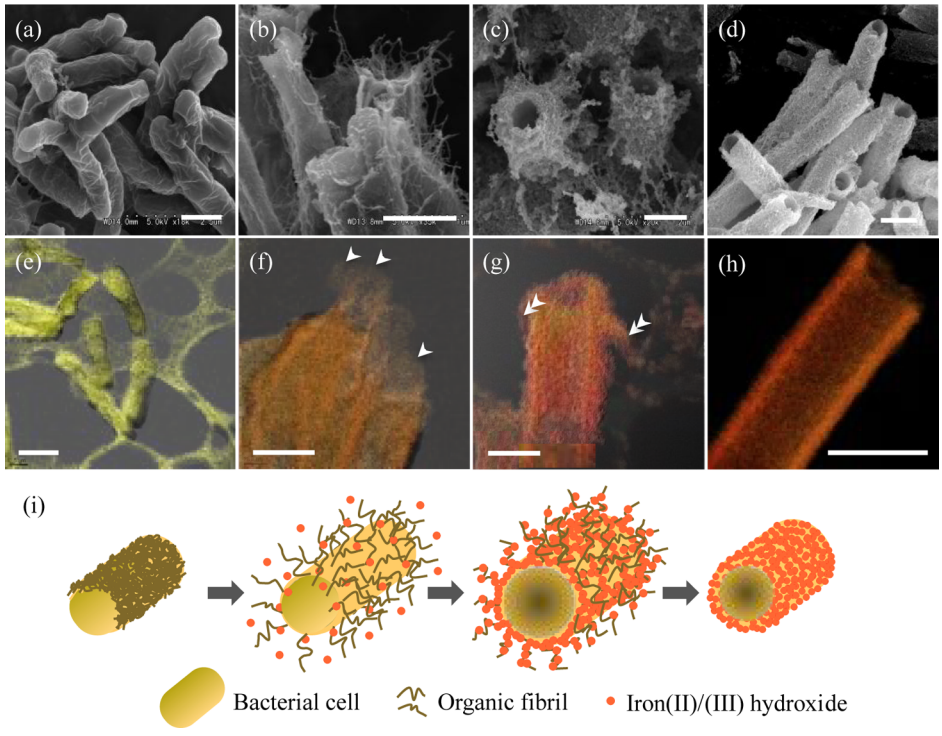

Figure 6. Time-series change in sheath appearances during the formation of metal-deposited cBIOX. (a−d) SEM images of the sheaths, which were chemically fixed immediately before being immersed in reaction (iron deposition) solutions (a) and after the deposition treatment for 24 h (b), 36 h (c), and 48 h (d) for electron microscopic analyses. (e−h) STEM-EDS elemental mapping images of the sheaths corresponding to (a−d), in which the maps for C (yellow) are overlayed with those for Fe (red). Arrowheads and double arrowheads indicate untied organic fibrils and fibrils with deposited iron oxides and additional metals, respectively. Scale bars are 1 μm. (i) Schematic representation of sequential sheath appearances in the course of BIOX formation.

https://dx.doi.org/10.1021/acsomega.0c03574
ACS Omega 2020, 5, 27287−27294

previously.[32] The additional metallic elements are supposed to be codeposited during this period. In the third event, as the deposition process proceeded, the fibrils with deposited iron oxides and additional metals gradually thickened and the sheath bodies swelled toward the outside (Figure 6c,g, the third diagram from the left in Figure 6i). It is thus inferred that the hollowing event was promoted via a release of cellular contents along with the swelling of whole sheath bodies. In the last event, the iron oxide- and additional metal-deposited fibrils were weaved into a tubular shape, and the sheath surface turned a wheal-like mesh pattern (Figure 6d,h, the rightmost diagram in Figure 6i). Takeda et al. proposed that the assembly of sheath fibrils is attributed to the formation of disulfide bonds between L-cysteine residues contained in side chains of the fibrils in *L. cholodnii* SP-6.[33] Given that the idea is applicable to our results, it is conceivable that such a reaction of disulfide bond formation occurs at this period via unknown oxidation states.

Although the BIOXs are attractive materials with unique physicochemical features, there have been challenges and difficulties in improvement of their functionalities. However, the breakthrough method refined in this study for development of novel cBIOXs would enable to improve the functionality of the material, according to the respective features of additional metallic elements deposited to the sheaths. In particular, we expect that the cBIOX-Zr and cBIOX-Ti are applicable for high-quality red pigments and high-performance scaffolds for cell cultures, respectively. Indeed, our preliminary experiments showed that heat-treated cBIOX-Zr30 products exhibited increased chroma and lightness (Figure S8). In addition, the two-step method allowed us to expand a range of metallic elements to be deposited onto the cBIOX sheaths. Kunoh et al. have recently reported direct evidence that the organic nanofibrils extracted from *Leptothrix* immature sheaths sorbed a variety of metallic elements with diverse sorption degrees.[34] It is therefore fascinating to execute encompassing screenings of metallic elements for deposition onto the cBIOX sheaths. In the meantime, the novel cBIOXs were experimentally produced almost completely under the control by artificial manipulations. Consequently, the present work would provide valuable information for a commercial-scale production of the bioderived material toward industrial applications.

CONCLUSIONS

In brief summary, we have successfully established the two-step method for production of novel cBIOX sheaths with depositions of various additional metals, including Al, Zr, and Ti. The elemental composition ratios in the additional element-containing cBIOXs were controllable optionally by changes in concentrations of the additive metal salts in the metal deposition process. STEM-EDS analysis showed that the additional metals are distributed uniformly in the microtubular sheaths, and the depositions of the metals do not affect the microstructure and amorphous state. Raman spectroscopy exemplified that the chemical linkage of Fe−O−Al is contained in the cBIOX-Al40 matrix. Time-course analysis of the cBIOX formation revealed that the process comprises four consecutive events, (i) untying of organic fibrils on primary sheaths, (ii) deposition of iron oxide nanoparticles and additional metals on organic fibrils, (iii) swelling and hollowing out of sheath bodies, and (iv) weaving and compaction of iron-deposited fibrils into tubular sheaths. The present work can contribute to creations of innovative BIOX materials with improved functionalities.

EXPERIMENTAL SECTION

L. cholodnii strain OUMS1 (NITE BP-860)[7] was used in this study after recovery on an SGP (silicon−glucose−peptone) agar plate medium[23] from frozen glycerol stocks. OUMS1 cells were inoculated to a small amount (∼20 mL) of SGP liquid medium and incubated in a rotary shaker for 3 days. The temperature and rotation speed of the shaker were 20 °C and 70 rpm, respectively, unless otherwise stated. After 3 days of incubation, aggregated lumps of bacterial cells were dispersed by passing the culture fluid through a 23-gauge needle, as described previously,[13] and were used as "precultured cells" for subsequent experiments.

Preparation of additional metallic element-containing BIOX sheaths was carried out by the two-step method, as simply shown in Figure 1a. In the first step, the precultured cells were inoculated to a large amount (∼250 mL) of SGP liquid medium and incubated in the rotary shaker for 3 days. Immature organic sheaths were recovered as precipitates by centrifugation at 2380*g*, for 10 min, and washed with a 10-fold volume of distilled water to remove trace medium components and bacterial secretions. In the second step, the immature organic sheaths were immersed in 20 mM acetate buffer (pH 4.0) containing 5 mg mL^{-1} iron powder (particle size 150 μm, Wako Pure Chemical Industries, Osaka, Japan) (hereafter referred to as an iron deposition solution) and incubated in the rotary shaker for 42 h. Then, each of the additive metallic compounds such as $AlCl_3$, $ZrCl_4$, and $TiCl_3$ (Nacalai Tesque, Kyoto, Japan) was added to the sheath suspension at various concentrations (1−10 mM), and the suspensions were further incubated for 24 h under the same conditions. The precipitate containing the BIOX sheaths was fractionated by decantation of the supernatant, washed with a 10-fold volume of distilled water, and lyophilized using a freeze dryer.

The BIOX sheaths produced were characterized using several analytical methods. The micromorphology and chemical compositions were examined by SEM (S-4300, Hitachi, Tokyo, Japan) coupled with EDX and transmission electron microscopy (TEM; JEM-2100F, JEOL, Tokyo, Japan). Elemental mapping images were acquired in the scanning TEM (STEM) mode with a CEOS Cs corrector, and high-resolution TEM images were acquired in the TEM mode. For time-course experiments, specimens were fixed with a mixture of 2.5% glutaraldehyde, 1% OsO_4, and 4.5% sucrose in 100 mM cacodylate buffer (pH 7.0) on ice for 2 h, followed by dehydration with a dilution series of ethanol and *tert*-butyl alcohol and freeze-drying, before analyzing by SEM and TEM. The crystallographic features were examined by ED analysis and powder XRD (RINT-2000, Rigaku, Tokyo, Japan) using Cu Kα radiation. Raman spectroscopy was carried out using a Raman laser spectrometer (NRS-5100NPS, JASCO, Tokyo, Japan) with an excitation wavelength of 532 nm.

ASSOCIATED CONTENT

Supporting Information

The Supporting Information is available free of charge at https://pubs.acs.org/doi/10.1021/acsomega.0c03574.

Growth curves of OUMS1 cells in the presence of Al, Ru, or Si; changes in Fe concentrations in iron powder-containing SGP medium and acetate buffer solution;

https://dx.doi.org/10.1021/acsomega.0c03574
ACS Omega 2020, 5, 27287−27294

micromorphology and elemental composition of Zr- and Ti-deposited BIOX sheaths; pore size distributions of mesopores and micropores in cBIOX-Al40 and cBIOX; pore size distributions of mesopores and micropores in cBIOX-Zr40 and cBIOX-Ti86; Raman spectroscopy of cBIOX-Zr and cBIOX-Ti samples; micromorphology of organic sheaths treated with or without a reducing agent; and color measurement of heat-treated cBIOX-Zr30 and cBIOX-Zr0 samples (PDF)

AUTHOR INFORMATION

Corresponding Authors

Katsunori Tamura − *Graduate School of Natural Science and Technology, Okayama University, Okayama 700-8530, Japan; Bengala Techno-Lab, Kawasaki-shi, Kanagawa 216-0007, Japan*; Phone: +81-86-251-8107; Email: ktamura@okayama-u.ac.jp; Fax: +81-86-251-8087

Jun Takada − *Graduate School of Natural Science and Technology, Okayama University, Okayama 700-8530, Japan*; Phone: +81-86-251-8107; Email: jtakada@okayama-u.ac.jp; Fax: +81-86-251-8087

Authors

Tatsuki Kunoh − *Graduate School of Natural Science and Technology, Okayama University, Okayama 700-8530, Japan*

Makoto Nakanishi − *Graduate School of Natural Science and Technology, Okayama University, Okayama 700-8530, Japan*

Yoshihiro Kusano − *Department of Applied Chemistry and Biotechnology, Okayama University of Science, Okayama 700-0005, Japan*; orcid.org/0000-0003-3646-3413

Complete contact information is available at: https://pubs.acs.org/10.1021/acsomega.0c03574

Author Contributions

K.T. designed the study, conducted most of the experiments, and wrote the manuscript; T.K. provided technical advice; M.N. performed Raman spectroscopy; Y.K. performed STEM-EDS; J.T. developed the original concept of the project.

Funding

This study was financially supported by the JST-CREST project (2012−2017) (J.T.).

Notes

The authors declare no competing financial interest.

ACKNOWLEDGMENTS

We thank Tomoko Suzuki, Keiko Toyoda, and Mika Yoneda for technical supports.

REFERENCES

(1) Emerson, D.; Fleming, E. J.; McBeth, J. M. Iron-Oxidizing Bacteria: an Environmental and Genomic Perspective. *Annu. Rev. Microbiol.* **2010**, *64*, 561−583.

(2) Kunoh, T.; Kunoh, H.; Takada, J. Perspectives on the Biogenesis of Iron Oxide Complexes produced by Leptothrix, an Iron-Oxidizing Bacterium and Promising Industrial Applications for their Functions. *J. Microb. Biochem. Technol.* **2015**, *07*, 419−426.

(3) van Veen, W. L.; Mulder, E. G.; Deinema, M. H. The Sphaerotilus-Leptothrix Group of Bacteria. *Microbiol. Rev.* **1978**, *42*, 329−356.

(4) Schmidt, B.; Sánchez, L. A.; Fretschner, T.; Kreps, G.; Ferrero, M. A.; Siñeriz, F.; Szewzyk, U. Isolation of Sphaerotilus-Leptothrix Strains from Iron Bacteria Communities in Tierra del Fuego Wetlands. *FEMS Microbiol. Ecol.* **2014**, *90*, 454−466.

(5) Takada, J.; Hashimoto, H. Characteristics of Biogenous Iron Oxide Microtubes Formed by Iron-Oxidizing Bacteria, Leptothrix ochracea. *Handbook of Metal Biotechnology*, 2012; Vol. *139*−*148*.

(6) Takeda, M.; Makita, H.; Ohno, K.; Nakahara, Y.; Koizumi, J.-i. Structural Analysis of the Sheath of a Sheathed Bacterium, Leptothrix cholodnii. *Int. J. Biol. Macromol.* **2005**, *37*, 92−98.

(7) Sawayama, M.; Suzuki, T.; Hashimoto, H.; Kasai, T.; Furutani, M.; Miyata, N.; Kunoh, H.; Takada, J. Isolation of a Leptothrix Strain, OUMS1, from Ocherous Deposits in Groundwater. *Curr. Microbiol.* **2011**, *63*, 173−180.

(8) Emerson, D.; Vet, W. D. The Role of FeOB in Engineered Water Ecosystems: A Review. *J. Am. Water Works Assoc.* **2015**, *107*, E47−E57.

(9) Hashimoto, H.; Asaoka, H.; Nakano, T.; Kusano, Y.; Ishihara, H.; Ikeda, Y.; Nakanishi, M.; Fujii, T.; Yokoyama, T.; Horiishi, N.; Nanba, T.; Takada, J. Preparation, Microstructure, and Color Tone of Microtubule Material Composed of Hematite/Amorphous-Silicate Nonocomposite from Iron Oxide of Bacterial Origin. *Dyes Pigm.* **2012**, *95*, 639−643.

(10) Hashimoto, H.; Kobayashi, G.; Sakuma, R.; Fujii, T.; Hayashi, N.; Suzuki, T.; Kanno, R.; Takano, M.; Takada, J. Bacterial Nanometric Amorphous Fe-Based Oxide: A Potential Lithium-Ion Battery Anode Material. *ACS Appl. Mater. Interfaces* **2014**, *6*, 5374−5378.

(11) Ema, T.; Miyazaki, Y.; Kozuki, I.; Sakai, T.; Hashimoto, H.; Takada, J. Highly Active Lipase Immobilized on Biogenous Iron Oxide via an Organic Bridging Group: The Dramatic Effect of the Immobilization Support on Enzymatic Function. *Green Chem.* **2011**, *13*, 3187−3195.

(12) Mandai, K.; Korenaga, T.; Ema, T.; Sakai, T.; Furutani, M.; Hashimoto, H.; Takada, J. Biogenous Iron Oxide- Immobilized Palladium Catalyst for the Solvent-Free Suzuki−Miyaura Coupling Reaction. *Tetrahedron Lett.* **2012**, *53*, 329−332.

(13) Emerson, D.; Ghiorse, W. C. Isolation, Cultural Maintenance and Taxonomy of a Sheath-Forming Strain of Leptothrix discophora and Characterization of Manganese-Oxidizing Activity Associated with the Sheath. *Appl. Environ. Microbiol.* **1992**, *58*, 4001−4010.

(14) Emerson, D.; Fleming, E. J.; McBeth, J. M. Iron-Oxidizing Bacteria: An Environmental and Genomic Perspective. *Annu. Rev. Microbiol.* **2010**, *64*, 561−583.

(15) Hedrich, S.; Schlömann, M.; Johnson, D. B. The Iron-Oxidizing Protobacteria. *Mycology* **2011**, *157*, 1551−1564.

(16) Emerson, D.; Ghiorse, W. C. Ultrastructure and Chemical Composition of the Sheath of Leptothrix discophora SP-6. *J. Bacteriol.* **1993**, *175*, 7808−7818.

(17) Emerson, D.; Ghiorse, W. C. Role of Disulfide Bonds in Maintaining the Structural Integrity of the Sheath of Leptothrix discophora SP-6. *J. Bacteriol.* **1993**, *175*, 7819−7827.

(18) De Vrind-de Jong, E. W.; Corstjens, P. L. A. M.; Kempers, E. S.; Westbroek, P.; de Vrind, J. P. M. Oxidation of Manganese and Iron by Leptothrix discophora: Use of N,N,N′,N′-Tetramethyl-p-Phenylenediamine as an Indicator of Metal Oxidation. *Appl. Envion. Microbiol.* **1990**, *56*, 3458−3462.

(19) Suzuki, T.; Ishihara, H.; Toyoda, K.; Shiraishi, T.; Kunoh, H.; Takada, J. Autolysis of Bacterial Cells Leads to Formation of Empty Sheaths by Leptothrix spp. *Minerals* **2013**, *3*, 247−257.

(20) Kunoh, T.; Nagaoka, N.; McFarlane, I.; Tamura, K.; El-Naggar, M.; Kunoh, H.; Takada, J. Dissociation and Re-Aggregation of Multicell-Ensheathed Fragments Responsible for Rapid Production of Massive Clumps of Leptothrix Sheaths. *Biology* **2016**, *5*, 32.

(21) Kunoh, T.; Hashimoto, H.; McFarlane, I.; Hayashi, N.; Suzuki, T.; Taketa, E.; Tamura, K.; Takano, M.; El-Naggar, M.; Kunoh, H.; Takada, J. Abiotic Deposition of Fe Complexes onto Leptothrix Sheaths. *Biology* **2016**, *5*, 26.

(22) Suzuki, T.; Ishihara, H.; Furutani, M.; Shiraishi, T.; Kunoh, H.; Takada, J. A Novel Method for Culturing of Leptothrix sp. Strain OUMS1 in Natural Conditions. *Minerals* **2012**, *2*, 118−128.

(23) Suzuki, T.; Kunoh, T.; Nakatsuka, D.; Hashimoto, H.; Tamura, K.; Kunoh, H.; Takada, J. Use of Iron Powder to Obtain High Yields of Leptothrix Sheaths in Culture. *Minerals* **2015**, *5*, 335−345.
(24) Nedkov, I.; Slavov, L.; Angelova, R.; Blagoev, B.; Kovacheva, D.; Abrashev, M. V.; Iliev, M.; Groudeva, V. Biogenic Nanosized Iron Oxides Obtained from Cultivation of Iron Bacteria from the Genus Leptothrix. *J. Biol. Phys.* **2016**, *42*, 587−600.
(25) Shopska, M.; Paneva, D.; Kadinov, G.; Cherkezova-Zheleva, Z.; Mitov, I.; Iliev, M. Study on the Composition of Biogenic Iron-Containing Materials Obtained under Cultivation of the Leptothrix sp. on Different Media. *Appl. Biochem. Biotechnol.* **2017**, *181*, 867−883.
(26) Ishihara, H.; Hashimoto, H.; Taketa, E.; Suzuki, T.; Mandai, K.; Kunoh, H.; Takada, J. Silicon-Rich, Iron Oxide Microtubular Sheath Produced by an Iron-Ooxidizing Bacterium, Leptothrix sp. Strain OUMS1, in Culture. *Minerals* **2014**, *4*, 565−577.
(27) Furutani, M.; Suzuki, T.; Ishihara, H.; Hashimoto, H.; Kunoh, H.; Takada, J. Assemblage of Bacterial Saccharic Microfibrils in Sheath Skeleton Formed by Cultured Leptothrix sp. Strain OUMS1. *J. Mar. Sci. Res. Dev.* **2013**, *3*, 001.
(28) Furutani, M.; Suzuki, T.; Ishihara, H.; Hashimoto, H.; Kunoh, H.; Takada, J. Initial Assemblage of Bacterial Saccharic Fibrils and Element Deposition to Form an Immature Sheath in Cultured Leptothrix sp. Strain OUMS1. *Minerals* **2011**, *1*, 157−166.
(29) Kunoh, T.; Matsumoto, S.; Nagaoka, N.; Kanashima, S.; Hino, K.; Uchida, T.; Tamura, K.; Kunoh, H.; Takada, J. Amino Group in Leptothrix Sheath Skeleton is Responsible for Direct Deposition of Fe(III) Minerals onto the Sheaths. *Sci. Rep.* **2017**, *7*, 6498.
(30) Ryan, J. N.; Gschwend, P. M. Extraction of Iron Oxides from Sediments Using Reductive Dissolution by Titanium (III). *Clays Clay Miner.* **1991**, *39*, 509−518.
(31) Liu, H.; Chen, T.; Zou, X.; Qing, C.; Frost, R. L. Effect of Al Content on the Structure of Al-Substituted Goethite: A Micro-Raman Spectroscopic Study. *J. Raman Spectrosc.* **2013**, *44*, 1609−1614.
(32) Kunoh, T.; Hashimoto, H.; Suzuki, T.; Hayashi, N.; Tamura, K.; Takano, M.; Kunoh, H.; Takada, J. Direct Adherence of Fe (III) Particles onto Sheaths of Leptothrix sp. Strain OUMS1 in Culture. *Minerals* **2016**, *6*, 4−19.
(33) Takeda, M.; Kondo, K.; Yamada, M.; Koizumi, J.-i.; Mashima, T.; Matsugami, A.; Katahira, M.; Katahira, K. Solubilization and Structural Determination of a Glycoconjugate Which is Assembled into the Sheath of Leptothrix cholodnii. *Int. J. Biol. Macromol.* **2010**, *46*, 206−211.
(34) Kunoh, T.; Nakanishi, M.; Kusano, Y.; Itadani, A.; Ando, K.; Matsumoto, S.; Tamura, K.; Kunoh, H.; Takada, J. Biosorption of Metal Elements by Exopolymer Nanofibrils Excreted from Leptothrix Cells. *Water Res.* **2017**, *122*, 139−147.

https://dx.doi.org/10.1021/acsomega.0c03574
ACS Omega 2020, 5, 27287−27294